Science World Publishing

Open Access Journal | Volume: 1.1

JOURNAL OF ADVANCED MATERIAL SCIENCE AND INNOVATIONS

Nano-sized Laser Beams without Diffraction Spreading

Yikuan Wang

College of Physics and Electrical Engineering, Yancheng Teachers University, Jiangsu Province, 224007 People's Republic of China

Article Information

Article Type: Original Article
Journal Type: Open Access
Volume: 1 **Issue:** 1
Manuscript ID: JAMSI-1-101
Publisher: Science World Publishing

Received Date: 09 March 2020
Accepted Date: 28 March 2020
Published Date: 10 April 2020

***Corresponding author:**

Yikuan Wang

College of Physics and Electrical Engineering
Yancheng Teachers University
Jiangsu Province
224007 People's Republic of China
Email: yikuanw@gmail.com

Citation: Yikuan Wang (2020) Nano-sized Laser Beams without Diffraction Spreading. J Adv Mater Sci Innov, 1(1);1-4

ABSTRACT

Whereas exciting progress has been made to beat diffraction in optical spectroscopy [1-8], making a nano-sized laser beam remains challenging due to diffraction spread [9,10]. Using Bethe's expression for the optical transmission coefficient of a circular hole in a perfect conductor screen of zero thickness [9,11]. $T=1024\pi^3a^6/27\lambda^4$, we found that the transmission of light with a wavelength λ=800 nm through such a circular hole of a radius of 1 nm is about ~2.3×10^{-6}. So a decent nanosized laser beam for miniaturization of optical elements is not available. Here we show that coupling Surface Plasmon-Polaritons (SPPs) to appropriate dielectric material can result in fundamentally diffraction-free down-sized, especially nano-sized laser beams. For example, the composite structure Si_3N_4/Au(44.5nm)/SiO_2 (456nm)/(SiO_2, Si_3N_4, SiO_2) can achieve a nano-sized laser beam of about half the incoming light intensity. This approach, by transforming the macroscopic laser beams into multiple nano-sized laser beams, holds promise for ultrafast laser imprinting of nanopores for DNA sequencing and other miniature photonic devices in optical signal processing industries.

KEYWORDS

Optical spectroscopy, Nano-sized Laser Beams, DNA sequencing

INTRODUCTION

In optics, diffraction renders a blurred Airy disk image for a point object and thus creates a resolution limit to an imaging instrument [1]. Over the past decades, tremendous progress has been made to improve the resolutions of optical images. Hell et al. used a depletion laser beam to squeeze the non-depleted excitation fluorescent spot to a tiny point and achieved a 35 nm resolution of molecule images [2,3]. Zhuang et al. reconstructed 20 nm-resolution images of individual photo-switchable fluorescent molecules that are turned on and off by excitation light of different colors [12]. Betzig et al. used photo-activated localization microscopy to image intracellular proteins at a nanometer resolution [5]. Pendry proposed to use survived evanesce waves in negative-index media to make a perfect image [6], which was realized experimentally by Zhang et al., [7]. Yablonovitch et al. developed a 3D tapered metal-insulator-metal nano-gaped device that delivers background-free near-field images with a deep sub-wavelength resolution.

While these landmark advances are impressive in beating diffraction in image optics, overcoming the diffraction spreading of a laser beam is rarely studied. Light from a sub-wavelength aperture usually diffracts in all directions, which makes a nano-sized laser beam virtually impossible [9]. Townes et al. first discussed the possible suppression of rapid diffraction- spreading of a laser beam in nonlinear dielectric media by an intense laser [10]. Lezec et al. created an almost-directional light beam out of metallic films of a bull's eye structure, whose practical application is limited by the complicated fabrication of periodic grooves [13]. Noticing the importance of beating diffraction in science [1-8], here we propose an approach to make a nano- ized laser beam for technological applications

TRANSFER MATRIX MODELLING

We use a planar metal-dielectric tri-layer film to absorb laser light as SPPs at a conductor/dielectric interface [14,15] and add another top dielectric layer to reduce SPPs to free- space optical waves. This conversion does allow photons traveling directionally without diffraction [16].

We calculate the intensity of light reflected by and transmitted through this coupling structure [17-21] with a transfer-matrix method. The transfer-matrix method is briefly summarized as follows. Suppose the coupling structures are composed of optically isotropic and homogeneous N planar layers. Each layer i has a thickness di. Both the width of the first layer and that of the last layer are assumed to be infinite. The dielectric properties of each layer i are characterized by its complex dielectric functions $\varepsilon_i(\omega)$.

We use the dielectric functions calculated from the refractive index of materials (https://www.filmetrics.com/refractive-index-database). A p-polarized monochromatic plane wave with wavelength λ_0 is incident on the stack from layer 1 through layer N, making an arbitrary angle of incidence θ_1 with respect to the surface normal of the first interface. We describe the electric field in layer *i* as a superposition of the reflected and transmitted plane waves. For example, for a single ideal interface at the O-xy plane, the electric field below and above this interface is written as $\mathbf{E}(x,z<0)=\mathbf{E}e^{i}(k1_x x+k1_z z-wt)+\mathbf{E}'ei(k1_x x-k1_z z-wt)$ and $E\,(x,z>0)=\mathbf{E}e^{i}(k2_x x+k2_z z-wt)+\mathbf{E}'e^{i}(k2_x x-k2_z z-wt)$. Here the wave-vector for the incident plane wave is $k_{1x}\,\mathbf{i}+k_{1z}\,\mathbf{k}$, the wave-vector for the reflected plane wave is $k_{1x}\,\mathbf{i}+k_{1z}\,\mathbf{k}$ in layer 1, and so on for the wave-vectors in layer 2. The x-components of all the wave-vectors are equal, i.e., $k_{1x}=k_{2x}=\ldots k_{Nx}=2\pi n_1\, sin\theta_1/\lambda_\circ$. The z-components of the wave-vectors can be written as $k_{iz}=2\pi\sqrt{\varepsilon_i-\varepsilon_1\sin^2\theta_1}/\lambda_\circ$. The transformation of the incident and reflected fields across each interface *i* of two neighboring *i*-th and (*i*+1)-th layers are related to each other by an interface transfer matrix T(*i*), i.e.,

$$\begin{bmatrix} E_{(i+1)x} \\ E'_{(i+1)x} \end{bmatrix} = T(i)\begin{bmatrix} E_{ix} \\ E'_{ix} \end{bmatrix} \text{ with}$$

$$T(i)=\tfrac{1}{2}\begin{bmatrix} 1+\dfrac{\varepsilon_i k_{(i+1)z}}{\varepsilon_{(i+1)}k_{iz}} & 1-\dfrac{\varepsilon_i k_{(i+1)z}}{\varepsilon_{(i+1)}k_{iz}} \\ 1-\dfrac{\varepsilon_i k_{(i+1)z}}{\varepsilon_{(i+1)}k_{iz}} & 1+\dfrac{\varepsilon_i k_{(i+1)z}}{\varepsilon_{(i+1)}k_{iz}} \end{bmatrix} \quad (1)$$

Similarly, when the optical fields travel in a single j-th layer of thickness dj, the field amplitudes in the upper- and down-sides of this layer are related by a propagation transfer matrix T(dj), i.e.

$$\begin{bmatrix} E_{jx}(z_j=d_j+z_{j-1}) \\ E'_{jx}(z_j=d_j+z_{j-1}) \end{bmatrix} = T(d_j)\begin{bmatrix} E_{jx}(z_j=z_{j-1}) \\ E'_{jx}(z_j=z_{j-1}) \end{bmatrix}, \text{ with}$$

$$T(d_j)=\begin{bmatrix} e^{ik_{2z}d_j} & 0 \\ 0 & e^{-ik_{2z}d_j} \end{bmatrix} e^{ik_{zx}d_j\ tg\theta_2} \quad (2)$$

For a multilayer film, the electric fields at the first interface are related to those at the last interface by an overall T-matrix, which is the successive matrix products of the propagation transfer matrix and interface transfer matrix, i.e.,

$$\begin{bmatrix} E_{N-1x}(z_{N-1}=d_{N-1}+z_{N-2}) \\ E'_{N-1x}(z_{N-1}=d_{N-1}+z_{N-2}) \end{bmatrix} = T_{total}\begin{bmatrix} E_{1x}(z_1=0) \\ E'_{1x}(z_1=0) \end{bmatrix},$$

Where,

$$T_{total}=T(N-1)T(d_{N-1})\cdots T(3)T(d_3)T(2)T(d_2)T(1). \quad (3)$$

If we set the incident and reflected electric field from the bottom-most layer as one and r = E'1 / E1 and the transmitted and reflected field from the top-most layer as t = EN/E1 and 0, the matrix relation can then be expressed as:

$$\begin{bmatrix} t\cos\theta_N \\ 0 \end{bmatrix} = \begin{bmatrix} T_{11} & T_{12} \\ T_{21} & T_{22} \end{bmatrix}\begin{bmatrix} \cos\theta_1 \\ r\cos\theta_1 \end{bmatrix} \quad (4)$$

Thus the transmission and reflection coefficients of the final layer are given by

$$t=(T_{11}-T_{12}T_{21}/T_{22})\cos\theta_1/\cos\theta_N \quad (5)$$

and

$$r=-T_{21}/T_{22} \quad (6)$$

Finally, the reflectance R, the transmittance T, and the absorbance A are then given by R = | r² |,

$$T=\mathrm{Re}\left\{\frac{\mathbf{n}_N\cos\theta_N}{\mathbf{n}_i\cos\theta_i}\right\}|t|^2 \quad \text{and} \quad A=1-R-T$$

REFLECTANCE AND TRANSMITTANCE OF METAL-DIELECTRIC FILMS

We use this transfer matrix method to design our material structure. At first, we use a tri- layered film $Si_3N_4/Au/SiO_2$ stack to absorb laser light into SPPs with Kretschmann prism coupling configuration [22]. As shown in Figure 1, the 800 nm wavelength laser light with an angle of incidence is 49.1° is completely trapped at the interface of this film if the thickness of the smooth gold film [23] is about 44.5 nm.

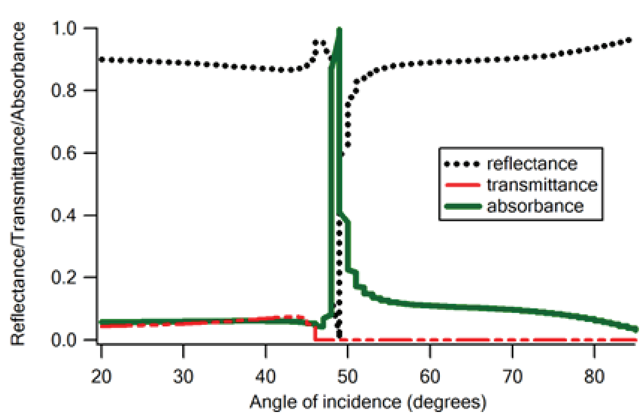

Figure 1: The reflectance, transmittance, and absorbance of the film Si_3N_4/Au(44.5nm)/SiO_2 stack vs the angle of incidence. The p-polarized monochromatic light with wavelength 800 nm casts on the film. The surface Plasmon resonance angle is found to be θ_{SPP}=49.1°.

We then put another Si_3N_4 layer onto the Si_3N_4/Au(44.5nm)/SiO_2 film with varying SiO_2 thickness. As shown in Figure 2, the transmittance of the film Si_3N_4/Au(44.5nm)/SiO_2/Si_3N_4 is 0~45.8% when the same light incident on it with the same angle of incidence. SPPs can couple efficiently with Si_3N_4 with a maximum transmittance of 45.8% in the sample Si_3N_4/Au(44.5nm)/SiO_2(456nm)/Si_3N_4.

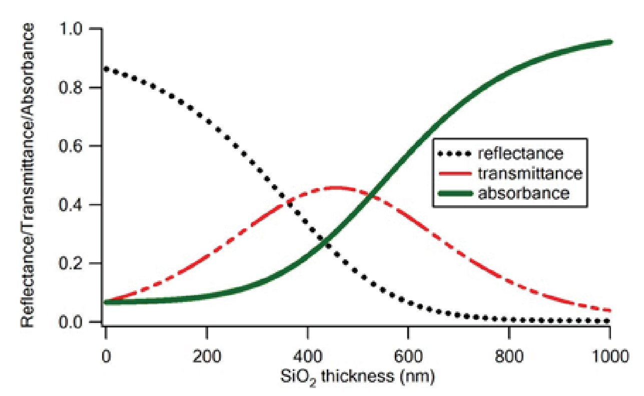

Figure 2: The reflectance, transmittance, and absorbance of Si_3N_4/Au(44.5nm)/SiO_2/Si_3N_4 film vs SiO_2 thickness. When p-polarized wavelength 800 nm light with casts on the sample Si_3N_4/Au(44.5nm)/SiO_2(456nm)/Si_3N_4 with an angle of incidence is θ_{SPP}=49.1°, the maximum transmittance is about 45.8%.

To understand the physics for this optical transmission, we also calculate the magnetic field in the i-th layer of the sample Si_3N_4/Au(44.5nm)/SiO_2(456nm)/Si_3N_4, which takes the following form.

$$H_{yi} = \omega\varepsilon_i(E_{ix} - E'_{ix})/k_{iz} \quad (9)$$

Here the x-components of the electric fields, including both the incident electric fields and the reflected electric fields in each layer, are also calculated by the transfer matrix formulation (3-6). As shown in Figure 3, the magnetic field amplitude reaches a maximum at the Au/SiO_2 interface and decays exponentially in the SiO_2 layer as plasma-polaritons. When entering the SiO_2/Si_3N_4 interface, the magnetic field stops declining and starts to travel through the Si_3N_4 layer as an un- attenuated oscillation. The SiO_2/ Si_3N_4 interface acts as an excitation source for this un- attenuated oscillation. This interface behaves just like shaking one end of a rope to generate a transverse string wave in the entire rope. This emission of light is self-directional, i.e., is diffraction-free, and is quite different from surface plasmon-coupled emission [24], or direction- selective emission in the metal-dielectric-metal structure [25] or light-beaming caused by the interaction of SPPs with surface grooves in the metal [13], or perfect transmission of light through pinholes in a Fabry-Perot cavity [26]. The top dielectric layer acts as a vent for SPP photons to emit, and the more surface area of the dielectric, the more free photons one can get.

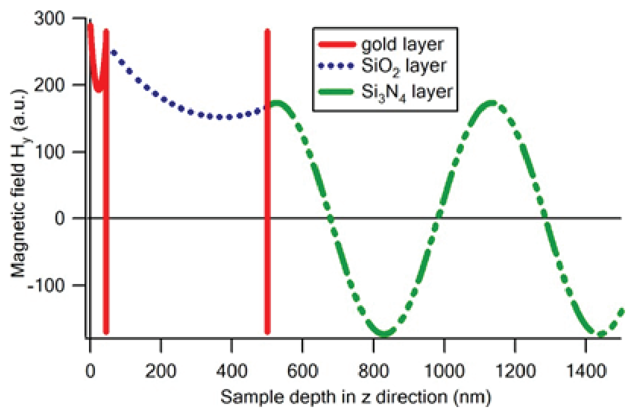

Figure 3: The magnetic field Hy in the sample Si_3N_4/Au(44.5nm)/SiO_2(456nm)/Si_3N_4 vs. sample depth. The magnetic field amplitude reaches the maximum at the Au/SiO_2 interface and then decays exponentially in the SiO_2 layer to form plasma polarities. When entering the SiO_2/ Si_3N_4 interface, the magnetic field in the SiO_{21} stops declining and starts to travel through the Si_3N_4 layer as un-attenuated oscillations.

This dielectric/metal/dielectric/dielectric structure can modify the wave-fronts of electromagnetic waves by the top dielectric material to turn laser light on and off simultaneously. For example, composite structure Si_3N_4/Au(44.5nm)/ SiO_2(456nm)/ (SiO_2, Si_3N_4, SiO_2) is obtained by sideway connecting the SPP structure Si_3N_4/Au(44.5nm)/ SiO_2 with the coupling structure Si_3N_4/Au(44.5nm)/SiO_2(456nm)/ Si_3N_4, as shown in Figure 4. This composite structure can trap most SPP photons at the gold-silicon interface, and a certain amount of SPPs becomes propagating photons in the capping layer Si_3N_4. Since SPPs scatter along with the interface when entering the lateral Si_3N_4/SiO_2 boundary, this SPP-scattering does not affect the far-field emission at all [27]. Therefore the beam size of this light transmission depends solely on the contact surface area of the top dielectric. One would expect the cross-section area of the resultant laser beam is the contact area of the topping dielectric material multiplied by a factor of sinθ1. So this structure is expected to make an optical beam of a few nanometers with no diffraction spreading. For example, if the contact area of the coupling layer Si_3N_4 is a few nanometers square and the thickness of SPP hosting layer SiO_2 is 456 nm thick, the incident laser could become a nano-sized laser beam with a tremendous transmittance of 45.8%.

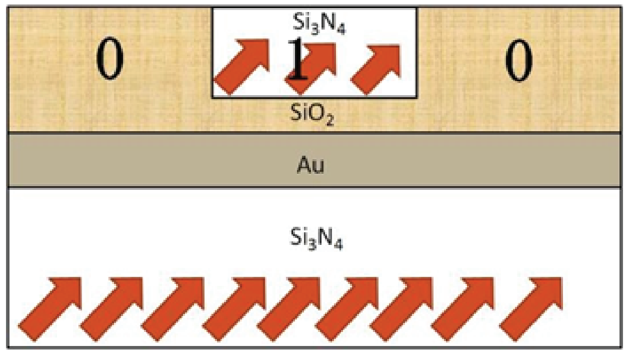

Figure 4: The light is partially turned on and off in the composite structure Si_3N_4/Au(44.5nm)/ SiO_2(456nm)/ (SiO_2, Si_3N_4, SiO_2). The beam size of this dielectric-coupled SPP emission depends solely on the contact area of the top dielectric coupling layer Si_3N_4, which turns the light on (hence it stores a bit “1”)

CONCLUSIONS

In summary, we performed a systematic study of the optical properties of SPP nanostructures coupled with dielectric materials. While this study has not been experimentally realized, there is no theoretical obstacle to build a diffraction-free laser beam by coupling SPP nanostructures with appropriate dielectric material. The capping layer alignment shows significant flexibility in building structures of interest in a variety of applications. The generation of multiple beams from a single laser source could be used to design new optical storage for fast batch-bit access in big-data industries, or to develop new 3D-printing technology to fabricate nano-porous membranes or nanofibers for efficient industrial-scale hydrogen generation [28] and CO_2 electrolysis for global dioxide emission reduction [29-31]. The merit of this diffraction suppression is that a decent nano-sized laser beam could be made possible. A continuous effort aiming at improving the optical field [32,33] of this sub-wavelength laser beam for the fabrication of a solid-state nanopore for DNA sequencing [34-37] is also possible.

BIBLIOGRAPHY

1. A. Pertsinidis, Y.X. Zhang, S. Chu. Subnanometre single-molecule localization, registration and distance measurements. Nature. 2010;466:647-U611.
2. S.W. Hell, J. Wichmann. Breaking the Diffraction Resolution Limit by Stimulated-Emission: Stimulated-Emission-Depletion Fluorescence Microscopy. Optics Letters. 1994;19:780-782.
3. V. Westphal, S.W. Hell, Nanoscale resolution in the focal plane of an optical microscope. Physical Review Letters. 2005;94:143903.
4. M.J. Rust, M. Bates, X. Zhuang. Sub-diffraction-limit imaging by stochastic optical reconstruction microscopy (STORM). Nat Methods. 2006;3:793-796.
5. E. Betzig, et al., Imaging Intracellular Fluorescent Proteins at Nanometer Resolution. Science. 2006;313:1642-1645.
6. J.B. Pendry, Negative Refraction Makes a Perfect Lens. Physical Review Letters 85, 3966-3969 (2000).
7. N. Fang, H. Lee, C. Sun, X. Zhang. Sub-Diffraction-Limited Optical Imaging with a Silver Superlens. Science. 2005;308:534-537.
8. W. Bao, et al., Mapping Local Charge Recombination Heterogeneity by Multidimensional Nanospectroscopic Imaging. Science. 2012;338:1317-1321.
9. H. A. Bethe, Theory of Diffraction by Small Holes. Physical Review. 1944;66:163-182.
10. R.Y. Chiao, E. Garmire, C.H. Townes, Self-Trapping of Optical Beams. Physical Review Letters. 1964;13:479-482.
11. C. Genet, T.W. Ebbesen. Light in tiny holes. Nature. 2007;445:39-

46.

12. S.W. Hell, J. Wichmann. Breaking the diffraction resolution limit by stimulated emission: stimulated-emission-depletion fluorescence microscopy. Optics Letters. 1994;19:780-782.
13. E. Betzig. Imaging intracellular fluorescent proteins at nanometer resolution. Science. 2006;313:1642-1645.
14. M.J. Rust, M. Bates, X. Zhuang. Sub-diffraction-limit imaging by stochastic optical reconstruction microscopy (STORM). Nature Methods. 2006;3:793-796.
15. H. J. Lezec, et al., Beaming light from a subwavelength aperture. Science. 2002;297:820-822.
16. S.A. Maier, H.A. Atwater. Plasmonics: Localization and guiding of electromagnetic energy in metal/dielectric structures. J Appl Phys. 2005;98:011101.
17. R. H. Ritchie. Plasma Losses by Fast Electrons in Thin Films. Physical Review. 1957;106:874-881.
18. Y. Wang. The on and off of optical waves in planar metal/dielectric stacks: potentials of making laser beams without diffraction spreading. 2016, pp. 56.
19. D.M. Whittaker, I.S. Culshaw. Scattering-matrix treatment of patterned multilayer photonic structures. Physical Review B. 1999;60:2610-2618.
20. S.G. Tikhodeev, A.L. Yablonskii, E.A. Muljarov, N.A. Gippius, T. Ishihara. Quasiguided modes and optical properties of photonic crystal slabs. Physical Review B. 2002;66:045102.
21. D.O.S. Melville, R.J. Blaikie. Analysis and optimization of multilayer silver superlenses for near-field optical lithography. Physica B: Condensed Matter. 2007;394:197-202.
22. W.J. Lee, J.B. You, K. Kwon, B. Park, K. Yu. Direction-selective emission with small angular divergence from a subwavelength aperture using radiative waveguide modes. Physical Review B. 2013;87:125108.
23. D. Lederman, et al., Magnetooptic properties of Fe/Pd and Co/Pd bilayers under hydrogen absorption. Applied Physics Letters. 2004;85:615-617.
24. E. Kretschmann, H. Raether. Radiative decay of nonradiative surface plasmons excited by light. Zeitschrift für Naturforschung A. 1968;23l:2135-2136.
25. J.S. Huang, et al., Atomically flat single-crystalline gold nanostructures for plasmonic nanocircuitry. Nature Communications. 2010;1:150.
26. J.R. Lakowicz. Radiative decay engineering 3. Surface plasmon-coupled directional emission. Analytical Biochemistry. 2004;324:153-169.
27. S. Hayashi, A. Maekawa, S.C. Kim, M. Fujii. Mechanism of enhanced light emission from an emitting layer embedded in metal-insulator-metal structures. Physical Review B. 2010;82:035441.
28. R. Merlin, Pinholes Meet Fabry-P\'erot: Perfect and Imperfect Transmission of Waves through Small Apertures. Physical Review X. 2012;2:031015.
29. T.A. Leskova, A.A. Maradudin, W. Zierau, Surface plasmon polariton propagation near an index step. Optics Communications. 2005;249, 23-35.
30. A. Landman, et al., Decoupled Photoelectrochemical Water Splitting System for Centralized Hydrogen Production. Joule. 2020;4:448-471.
31. W.A. Smith, T. Burdyny, D.A. Vermaas, H. Geerlings, Pathways to Industrial-Scale Fuel Out of Thin Air from CO₂ Electrolysis. Joule. 2019;3:1822-1834.
32. Q. Lu, F. Jiao. Electrochemical CO2 reduction: Electrocatalyst, reaction mechanism, and process engineering. Nano Energy. 2016;29:439-456.
33. Z. Yin, G.T.R. Palmore, S. Sun. Electrochemical Reduction of CO₂ Catalyzed by Metal Nanocatalysts. Trends in Chemistry. 2019;1:739-750.
34. S. Chu, J.E. Bjorkholm, A. Ashkin, A. Cable. Experimental-Observation of Optically Trapped Atoms. Physical Review Letters. 1986;57:314-317.
35. D.D. Awschalom, R. Hanson, J. Wrachtrup, B.B. Zhou. Quantum technologies with optically interfaced solid-state spins. Nature Photonics. 2018;12:516-527.
36. A. Ajoy, U. Bissbort, M.D. Lukin, R.L. Walsworth, P. Cappellaro. Atomic-Scale Nuclear Spin Imaging Using Quantum-Assisted Sensors in Diamond. Physical Review X. 2015;5:011001.
37. M.H. Abobeih, et al., Atomic-scale imaging of a 27-nuclear-spin cluster using a quantum sensor. Nature 576, 411-415 (2019).
38. A. Ashkin, J.M. Dziedzic, J.E. Bjorkholm, S. Chu. Observation of a Single-Beam Gradient Force Optical Trap for Dielectric Particles. Optics Letters. 1986;11:288-290.
39. D. Strickland, G. Mourou. Compression of amplified chirped optical pulses. Optics Communications. 1985;55:447-449.
40. P. Berini, I. De Leon. Surface plasmon-polariton amplifiers and lasers. Nature Photonics. 2012;6:16-24.
41. K. Itoh, W. Watanabe, S. Nolte, C.B. Schaffer. Ultrafast Processes for Bulk Modification of Transparent Materials. MRS Bulletin. 2011;31:620-625.
42. R.R. Gattass, E. Mazur. Femtosecond laser micromachining in transparent materials. Nature Photonics. 2008;2:219-225.
43. I.M. Derrington et al., Nanopore DNA sequencing with MspA. Proceedings of the National Academy of Sciences. 2010;107:16060-16065.
44. S. Agah, M. Zheng, M. Pasquali, A.B. Kolomeisky. DNA sequencing by nanopores: advances and challenges. Journal of Physics D: Applied Physics. 2016;49:413001.